Correction of Humidity Biases in Vaisala RS80-H Sondes during NAME

PAUL E. CIESIELSKI AND RICHARD H. JOHNSON

Department of Atmospheric Science, Colorado State University, Fort Collins, Colorado

JUNHONG WANG

Atmospheric Technology Division, National Center for Atmospheric Research, Boulder, Colorado

(Manuscript received 10 September 2008, in final form 13 February 2009)

ABSTRACT

Examination of the upper-air sonde data taken in conjunction with the North American Monsoon Experiment (NAME) revealed that data at several sites in the core monsoon region exhibited a significant dry bias. In this study, a simple, yet effective, statistical correction technique is applied to correct this dry bias. In addition, a second correction is applied to all Vaisala RS80-H sondes to remove a daytime dry bias resulting from solar heating of the humidity sensor. Moisture analyses computed from the corrected sondes compare favorably to those from independent satellite and aircraft estimates. The corrections led to significant improvement in the description of the humidity field and in several convective parameters, such as precipitable water (PW), CAPE, convective inhibition (CIN), and in the diurnal cycle of apparent drying Q_2.

1. Introduction

Recent concerns over climate change scenarios have made us aware of the need to create and maintain legacy atmospheric datasets. Such high-fidelity datasets have many important applications, including diagnostic studies, accurate initialization of models, calibration and validation of independent datasets, and verification of model output from case studies to climate simulations. Datasets from field programs are especially suited for these purposes, not only for their intensive observations in both space and time, but also because the large suite of instrument platforms typically deployed allows for cross-calibration that can greatly enhance the accuracy of the data.

With the goal to create high-quality field program datasets, several efforts have been undertaken in recent years to correct humidity biases identified in upper-air sounding datasets. For example, dry biases identified in Vaisala RS80 sondes and moist biases in VIZ sondes were corrected in the Tropical Ocean Global Atmosphere (TOGA) Coupled Ocean–Atmosphere Response Experiment (COARE) sounding dataset (Wang et al. 2002; Ciesielski et al. 2003). Recently, humidity correction schemes were applied to Vaisala RS80 sondes in the African Monsoon Multidisciplinary Analysis (AMMA) project (Nuret et al. 2008), and Vaisala RS92 sondes were applied to the Mirai Indian Ocean cruise for the Study of MJO-convection Onset (MISMO; Yoneyama et al. 2008). Comparison of the precipitable water (PW) computed from the corrected datasets to independent global positioning system (GPS) data show that these corrections have substantially improved the description of the water vapor field. The impact of such corrections has been shown to result in improved diagnostic analyses (Guichard et al. 2000; Ciesielski et al. 2003), better simulations of convection and improvements in NWP (Lorenc et al. 1996), and (presumably) datasets that are better suited for model validation.

During the North American Monsoon Experiment (NAME), the upper-air sounding network over the core monsoon region was enhanced by increasing the sonde frequency at several Mexican Weather Service [Servicio Meteorológico Nacional (SMN)] operational sites and by the addition of five sounding sites along the Gulf of California (GOC). All the sounding systems in Mexico during NAME used Vaisala RS80-H sondes, including the additional sites, four of which were systems developed and operated by the National Center for Atmospheric

Corresponding author address: Paul E. Ciesielski, Department of Atmospheric Science, Colorado State University, Fort Collins, CO 80523.
E-mail: paulc@atmos.colostate.edu

DOI: 10.1175/2009JTECHA1222.1

Research (NCAR) and a fifth system deployed on the R/V *Altair* (AL). Although all these sites used RS80-H sondes, those launched at most of the SMN sites exhibited a significant dry bias relative to the sondes from the four NCAR sites. In addition, a daytime dry bias attributed to solar heating of the RS80-H sonde humidity sensor, as reported in numerous recent studies (e.g., Wang and Zhang 2008; Cady-Pereira et al. 2008), was also observed.

The goal of this study is to improve the description of the upper-air water vapor analyses in NAME. In section 2, data sources used in this study are described and the dry bias of the SMN sondes is examined. In section 3, a simple, yet effective, statistical correction technique is described that constrains the statistics of the moisture fields at the problem SMN sites to be consistent with that observed at more reliable sites, primarily the NCAR sites. A procedure for removing the daytime dry bias is also discussed. Impacts of these corrections on various moisture-related analyses are presented in section 4, and the results are summarized in section 5.

2. Data sources and nature of moisture bias

Figure 1 shows the location the radiosonde sites during the NAME enhanced observing period (EOP) from 7 July to 15 August 2004. Although NAME technically started on 1 July, it was not until 7 July that all the NCAR sites were operational. During 10 intensive observing periods (IOPs; ~18 days), sites in the enhanced budget array (EBA; polygon in Fig. 1) increased their launch frequency from 4 to 6 times per day to sample the diurnal cycle. During the NAME EOP, five additional sounding sites were set up in the GOC. Four of these sites had NCAR systems: one GPS/Loran Atmospheric Sounding System (GLASS) at Loreto (LR) and three integrated sounding systems (ISS) at Puerto Penasco (PP), Kino Bay (KB), and Los Mochis (LM). The fifth system was on board the Mexican Navy AL located near the mouth of the GOC. For the NAME EOP, new Vaisala RS80-H sondes were purchased for all the NCAR sites, all sites within the EBA, and SMN sites Zacatecas (ZC) and Monterrey (MT). Although only the NCAR sites and AL recorded the sonde serial numbers from which the sonde age can be determined, to the best of our knowledge, it appears that the sondes used in NAME were all manufactured in early 2004 (A. Douglass and J. Meitín 2006, personal communication). Although the sonde system on the AL was operated by scientists and students from the United States, its moisture bias, as will been seen shortly, bears similar characteristics to those seen at the other GOC SMN sites. Thus, to simplify the discussion, AL will be referred to in the remainder of this paper as an SMN site.

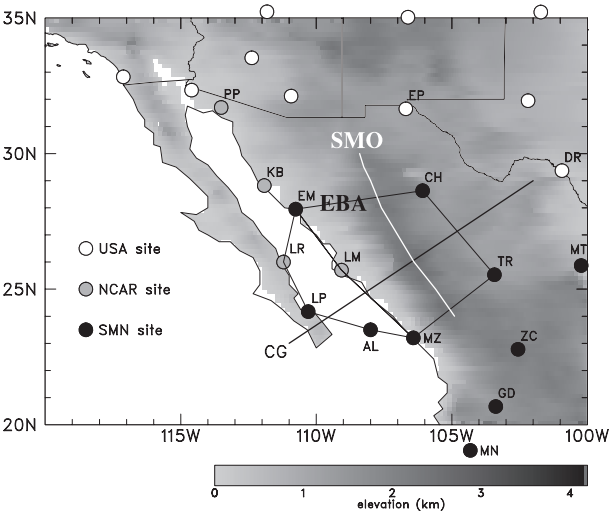

FIG. 1. Map of upper-air sounding sites during NAME with elevations shaded (elevation scale below). U.S. sites are denoted with white circles for EP and DR. NCAR sites are denoted with gray circles for PP, KB, LM, and LR. SMN sites are denoted with black circles for EM, CH, LP, AL, MZ, TR, MT, ZC, GD, and MN. The polygon denotes EBA, the white curve shows approximate location of SMO crest, and the black line shows the location of the cross-gulf (CG) transect shown in Fig. 14.

In this study, both native resolution sonde data as well as 5-hPa data are used. The native resolution of the data varied among the different sites: 1 s for the NCAR sites, 2 s for the SMN sites (including the AL), and 6 s for the U.S. sites. For ease of working with the sonde data, a uniform 5-hPa resolution sonde dataset was created for each site by interpolating temperature and moisture field to 5-hPa levels and averaging winds in 5-hPa layers. This 5-hPa resolution dataset was then subjected to a rigorous quality-control (QC) procedure described in Johnson et al. (2007). In a small percentage (~3%) of the NCAR sondes, the humidity sensor appears to become ice or water coated when passing through a cloud and does not recover (i.e., humidity remains saturated or nearly saturated for the remainder of its ascent). In these cases, IR geostationary brightness temperatures interpolated to the sounding locations were used to determine cloud-top heights, above which humidity values were flagged as questionable and not used in this study.

Constructed from the native high-resolution data, scatterplots of the surface water vapor mixing ratio r_s versus its value at the first point above the surface[1] r_{s+1} show distinctly different behavior at the SMN sites than at the ISS and U.S. sites (Fig. 2). It should be noted here

[1] This point ranges from ~5 m AGL at the NCAR sites, to ~10 m at the SMN sites, and 30 m at the U.S. sites.

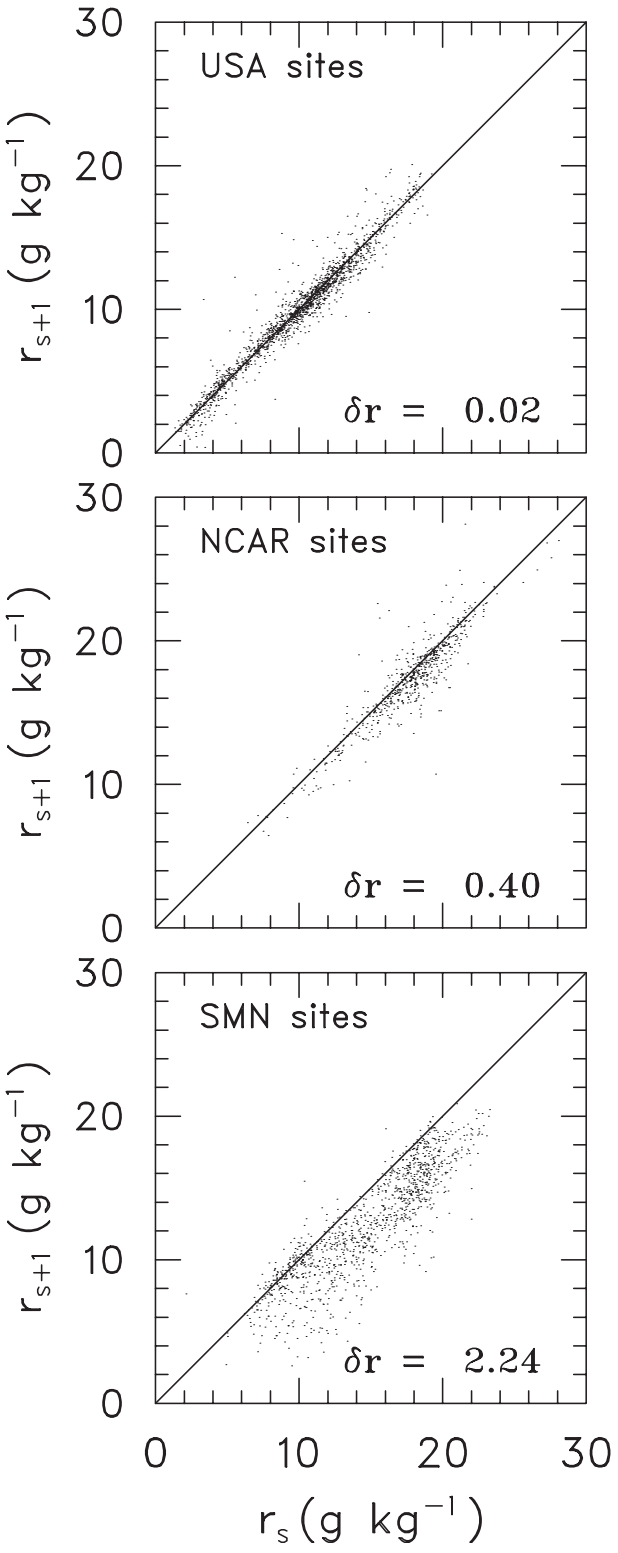

FIG. 2. Scatter diagrams of the water-vapor mixing ratio at the surface (r_s along x axis), with its value at first point above the surface r_{s+1} and the one-to-one reference line, for the (top) U.S., (middle) NCAR, and (bottom) SMN sites in Fig. 1. For each group of sites, the mean $\delta r = r_s - r_{s-1}$ is shown in lower right-hand corner.

that, except at LR and AL,[2] the sonde surface values are actually from a measurement made independent from the sonde. According to Stull (1988), observed r differences ($\delta r = r_s - r_{s+1}$) within the surface layer (10–100 m AGL) under all conditions of stability do not exceed a few tenths of a gram per kilogram. Although this is the case at the U.S. and NCAR sites, where the mean $\delta r < 0.5$, the mean δr at the SMN sites is considerably larger ($\delta r = 2.2$). Values of mean δr are somewhat larger in daytime sondes because of downward mixing of drier air into the top of mixed layer with day and night differences of 0.43 and 0.38 for the NCAR sites and 2.61 and 1.89 for the SMN sites, respectively.

Figure 3a shows the EOP-mean near-surface δr for individual SMN and NCAR sites. The NCAR sites along the west Mexican coast (KB and LM) have δr near 0.3, whereas the PP and LR sites, located in drier environments, have δr near 0.5. The mean δr from the individual U.S. sites (not shown) in Fig. 1 is 0.02. The small δr values at the NCAR and U.S. sites are in contrast to those observed at the SMN sites, which show that six of the sites have $\delta r \geq 2$. Although this analysis considers only the lowest few sonde points, it suggests that the majority of the SMN sites have a significant low-level dry bias. Torreon (TR), the SMN site located on the eastern slopes of the Sierra Madre Occidental (SMO), is an exception with a small mean δr (0.07), which is similar in magnitude to those of the U.S. and NCAR sites.

To examine the moisture bias further, the solid bars in Fig. 3b show the frequency of 5-hPa levels at SMN and NCAR sites that exhibit saturated conditions (i.e., RH $\geq$ 100% and computed with respect to ice for temperatures $<$0°C) using uncorrected data. Although these saturated layers occur throughout the troposphere, levels above 300 hPa account for about 40% of them, which is presumably related to large convective systems and their extensive stratiform anvils that move off the SMO. The frequency of saturated levels at the NCAR sites ranges from 1.2% at PP to 4.6% at LR and appears to vary roughly in relation to the distance of the sites from the SMO. In contrast, the SMN sites exhibit few, if any, saturated levels. From the inland SMN sites, TR has the highest frequency of saturated layers, albeit low compared to the NCAR sites. Despite the abundance of convective activity and clouds in this monsoonal region, the lack of saturation at the SMN sites indicates that a dry bias is likely present there to some degree.

[2] At AL, the only independent surface measurement used with the sondes was a pressure reading from a sensor on the ship's flux tower (P. Zuidema 2008, personal communication). At LR, the independent surface sensor was broken.

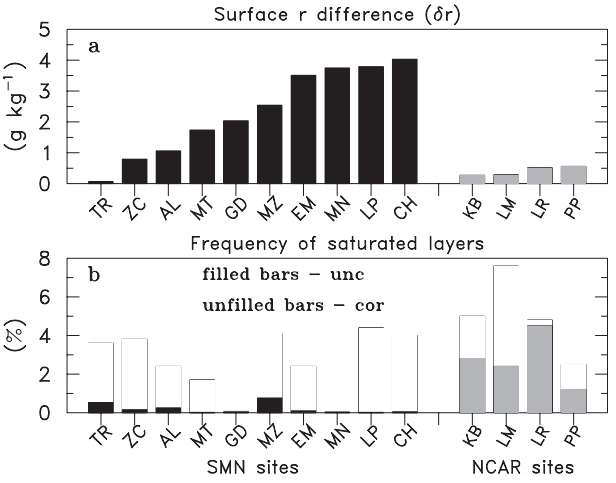

FIG. 3. (a) Mean δr (i.e., difference in r between the surface and the first point above surface) at SMN (black bars) and NCAR (gray bars) sites ordered from smallest to largest for each group of sites. (b) Frequency of 5-hPa saturated layers at SMN (black bars) and NCAR (gray bars) sites using data from surface to 100 hPa computed using uncorrected (filled bars) and corrected (unfilled bars) data.

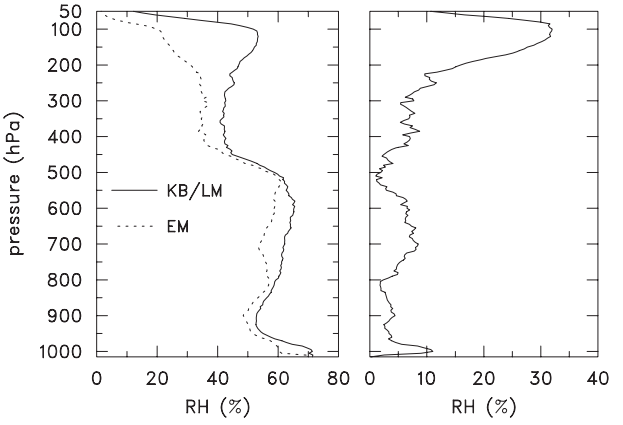

FIG. 4. (left) Mean RH profiles for merged KB–LM and EM sondes and (right) their difference. Profiles were computed using 109 contemporaneous sondes (i.e., launched within 2 h of each other at three sites).

Having established the presence of a dry bias in the SMN sites and the reasonableness of the data from the NCAR sites, we now intercompare 5-hPa sonde data at a few locations to determine the vertical structure of the SMN humidity bias. Ideally, such comparisons would involve collocated, contemporaneous SMN and NCAR sondes. As the next best alternative, these intercomparisons used sondes launched within 2 h of each other at sites that were in relatively close proximity to each other. Because Empalme (EM; an SMN site) lies between two NCAR sites (see Fig. 1), our first comparison uses a merged NCAR sonde in which RH values from KB and LM are weighted by their distance to EM, specifically $0.7 \times \text{KB} + 0.3 \times \text{LM}$. The 2-h time constraint resulted in the intercomparison shown in Fig. 4, which used 109 sondes from each site. Here, the mean RH profile from the merged KB–LM sonde is compared to the mean EM profile (left panel of Fig. 4) with their difference shown in the right panel of Fig. 4. The RH difference at the surface, which as noted earlier comes from independent measurements, is near zero. Within the boundary layer, RH at the SMN sites exhibits a 10% dry bias (or $\sim$2.5 g kg^{-1}) compared to the NCAR sites. Between the boundary layer and 300 hPa, the SMN dry bias varies between 2% and 8%. Above 300 hPa, the SMN dry bias peaks around 35% near 100 hPa. A second intercomparison between sites on the western Baja coast is shown in Fig. 5. In this case, the RH difference between 137 near-contemporaneous sondes at La Paz (LP; an SMN site) and LR (an NCAR site) shows a similar SMN dry bias to that in Fig. 4, suggesting that the dry biases at the SMN sites may have a common, yet undetermined, source.

Although no reliable NCAR sites are in close proximity to the inland higher-elevation SMN sites to determine the vertical structure of their humidity biases, it appears from the analysis presented in Figs. 2 and 3 that the quality of the humidity data at the TR site, for whatever reason, is better than that of the other SMN sites. On the other hand, the adjacent Chihauhau (CH) site, which is also on the windward eastern slopes of the SMO and at similar elevation (1124 and 1433 m for TR and CH, respectively) and distance from the SMO crest, exhibits the largest δr and likely the most serious dry bias of the SMN sites. Comparison of 147 near-contemporaneous sondes (Fig. 6) shows a significant RH dry bias (up to 10%) at CH relative to TR in the lowest layers and above 300 hPa.

Reasons for the dry bias depicted in Figs. 2–6 at the SMN sites are unclear. Because RH is a function of temperature, we examined temperature biases between NCAR and SMN sites but found them to be negligible ($\sim$0.1°C) and unable to account for any of the observed RH bias. As stated earlier, all sites in Mexico during NAME used relatively new Vaisala RS80-H sondes so that the most likely candidates for the dry bias at the SMN sites are poor prelaunch procedures and/or outdated ground station software.[3] On the other hand, the NCAR sites, which have more reasonable-looking data,

[3] In terms of ground station hardware, the SMN sites used Digicora systems at EM, LP, and MN; Digicora II systems at CH, GD, MZ, TR, and ZC; and the latest version of NCAR "in-house developed" hardware at the NCAR sites.

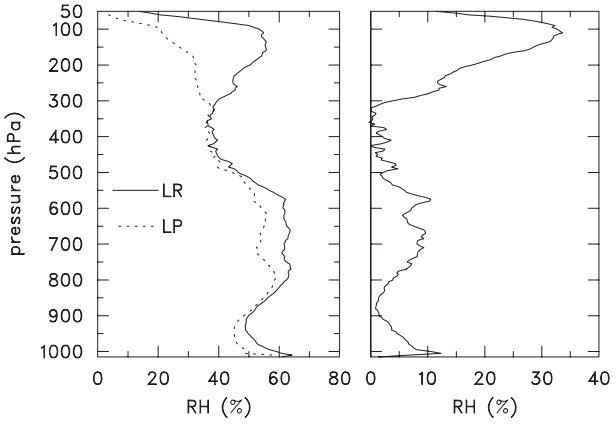

FIG. 5. (left) Mean RH profiles for LR and LP sondes and (right) their difference. Profiles were computed using 137 contemporaneous sondes (i.e., launched within 2 h of each other at two sites).

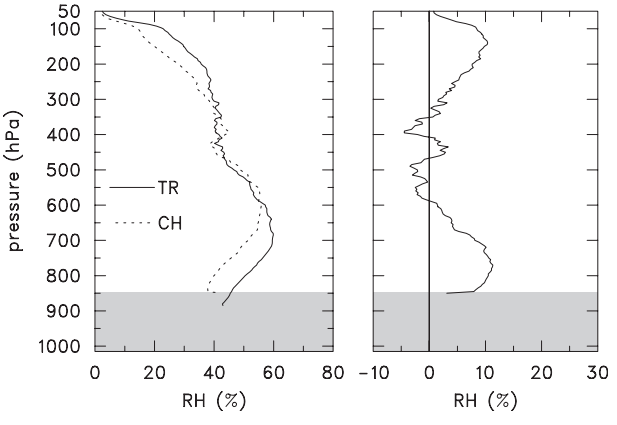

FIG. 6. (left) Mean RH profiles for TR and CH sondes and their difference. Profiles were computed using 147 contemporaneous sondes (i.e., launched within 2 h of each other at two sites). The shading indicates that these pressure levels were below ground.

were staffed by trained personnel using a standardized operating procedure and had the latest ground station processing software. In addition, regular inspections of each NCAR site were conducted during NAME to ensure that all instruments were functioning properly.

To help validate a moisture-correction scheme, it is useful to have an independent measurement of humidity such as PW estimates from satellites or ground-based GPS. Estimates of PW from GPS (Bevis et al. 1992) have an accuracy at midlatitudes of 1–2 mm (Rocken et al. 1995; Bock et al. 2007). During NAME, a network of seven GPS receivers was deployed over northwestern Mexico, predominantly in the state of Sonora, to measure PW (Kursinski et al. 2008). In their study, which compared global radiosonde PW estimates to ground-based GPS measurements, Wang and Zhang (2008) used only sounding sites that were located within 50 km of GPS receivers. This ensured that both sensors were detecting similar atmospheric domains. Unfortunately, only one GPS receiver in NAME satisfied this 50-km criterion; it was located on the northern GOC coast and about 5 km from the inland PP sonde site.

A second source of PW estimates used in this study is from the Atmospheric Microwave Scanning Radiometer for Earth Observing System (AMSR-E) retrievals. Away from land and rainy scenes, where microwave retrievals have difficulties, Wentz (1997) has shown that satellite microwave PW estimates have an accuracy of 1–2 mm. The nominal AMSR-E overpass times are at 0300 and 1500 LT over NAME region. Figure 7 shows the PW analysis based on AMSR-E retrievals for our region of interest averaged over the NAME EOP. Even with the masking over land areas, one can clearly see a peak in PW over the southeastern GOC which decreases northward and westward. For this study, version 5 AMSR-E PW data were obtained from the Remote Sensing Systems Web site (available online at http://www.remss.com).

A final source of moisture data independent from the sondes comes from 10 flights of an NOAA WP-3D research aircraft that were conducted during the NAME EOP from 8 July to 3 August. This aircraft was equipped with a Rosemount deiced model 102CP2AF temperature sensor (accuracy of 0.6°C), and an EdgeTech Vigilant model chilled mirror hygrometer (dewpoint temperature accuracy of 0.2°). The primary objective of these flight missions was to measure the moisture flux into and out of the NAME domain (Higgins et al. 2006). All flights occurred in the lower troposphere (i.e., generally below 700 hPa) during daylight hours, leaving and returning to Mazatlan (MZ), typically starting around 0700 LT and lasting 6–7 h. At least once during each flight, the aircraft flew over the position of AL, as seen in the flight on 24 July (Fig. 8). The aircraft measured thermodynamic and wind fields at 1-s intervals. To better facilitate a comparison with 5-hPa resolution sonde data, the aircraft data were averaged into 1-min means.

3. Humidity correction scheme

In this section, two separate humidity corrections are considered. The first correction procedure, referred to here as the cumulative distribution function (CDF) matching method (referred to as the CDF correction), attempts to adjust the statistical properties of questionable data from one site to those of good data from a nearby site. The RH intercomparisons shown in Figs. 4–6 form the basis for the CDF matches in this

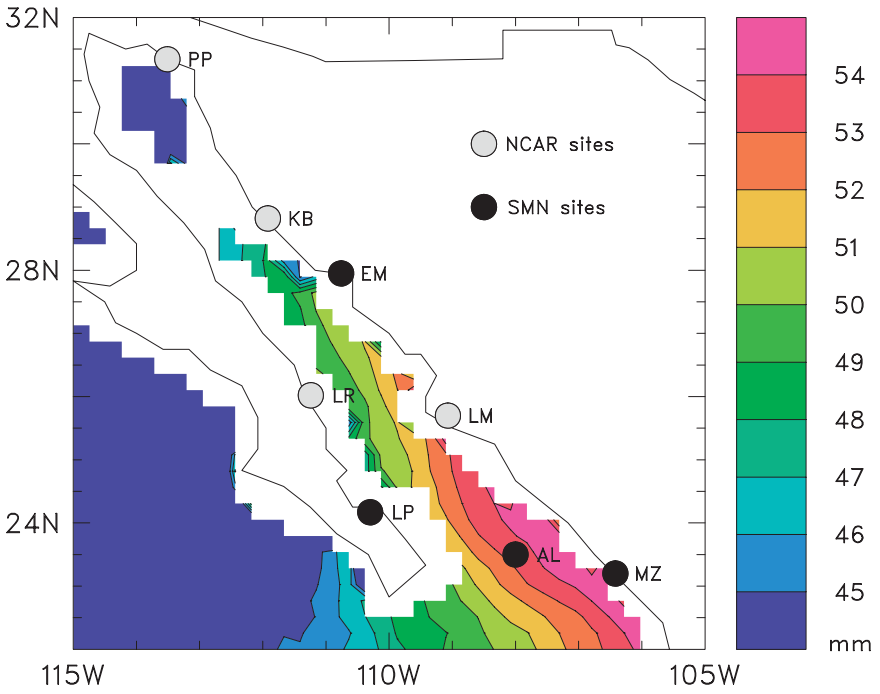

FIG. 7. PW analysis based on AMSR-E retrievals for NAME EOP with NCAR and SMN sites indicated with gray and black circles, respectively. Note that PW estimates from satellite microwave radiometers over land and coast are not provided because of difficulties in the retrieval schemes over these regions.

section. The second correction, applied to all sites (SMN, NCAR, and the United States) in the NAME domain using Vaisala sondes, is designed to remove the daytime dry bias observed in Vaisala sondes resulting from direct and indirect solar heating of the humidity sensor.

An underlying premise of this two-part correction scheme is that the nighttime Vaisala RS80-H sondes used at the NCAR sites are bias free because no corrections are applied to these sondes. This assumption is not necessarily valid because, as noted in the global analysis of GPS versus sonde PW comparisons (Wang and Zhang 2008), there is a slight mean dry bias (−0.35 mm) in nighttime Vaisala RS80-H sondes with a large site-to-site variance. Their study also shows that the dry bias in this sonde type is a function of total column PW with the bias being largest in drier conditions and little to no bias for PW > 40 mm. Because the SMN sites are corrected to the standard of the NCAR sites, after application of all corrections in this study, one might expect a small nighttime dry bias to be present. In addition, the analysis of Wang and Zhang (2008) suggests that this dry bias would likely be larger at sites with lower PW, such as PP and the mountain locations of CH and TR. As noted in section 4, this appears to be the case at PP, where GPS PW is available to quantify the sonde bias.

a. The CDF correction

The basis for this correction procedure is the assumption that near-homogenous atmospheric conditions exist between sites because of their proximity to each other and/or similar environments; thus, they exhibit similar statistical properties in their fields. First, we consider sites from coastal locations within the GOC. During the NAME period, low-level conditions in the GOC were characterized by mean southeasterlies with a robust land–sea breeze circulation along the coasts (Ciesielski and Johnson 2008). A fairly uniform SST field was present over the GOC in which offshore SSTs for the sites considered here were ~30°C, except at LP, where SSTs were about 1°C cooler (see Johnson et al. 2007, Fig. 7). Moisture conditions in this region varied more rapidly in an east–west direction as noted in AMSR-E PW analysis over this region (Fig. 7). Influenced more by the cool water of the northeast Pacific, locations on the west side of the GOC exhibited drier conditions than those on east side, which were impacted more by convective systems propagating off the SMO. For this reason, a bias correction is developed separately for sites along each coast.

The RH bias correction for sites on the east side of the GOC used a weighted combination of the KB and LM

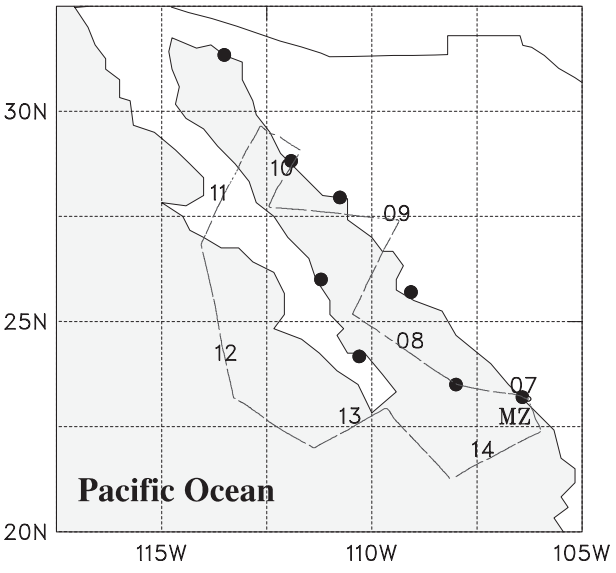

FIG. 8. Flight track for the NOAA WP-3D research aircraft on 24 Jul 2004. Numbers along the flight track indicate approximate local time at that location. The flight originated and terminated at MZ. Circles indicate the locations of sounding sites along GOC.

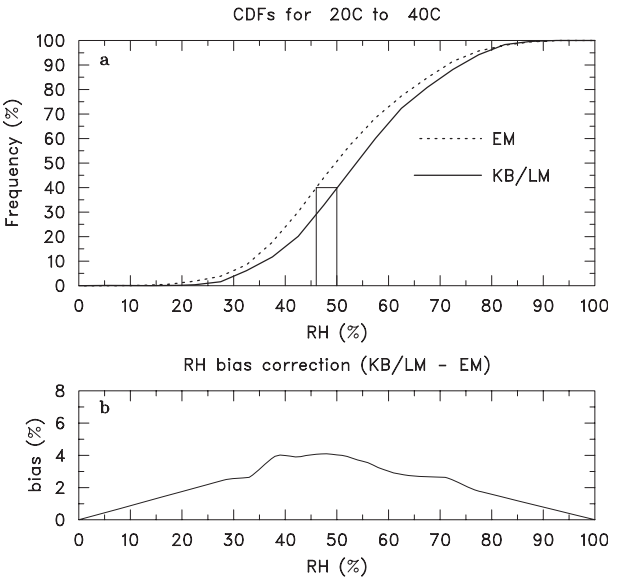

FIG. 9. (top) The cumulative distribution functions of RH for EM (dashed curve) and merged KB–LM (solid curve) data in the temperature range of 20°–40°C. Lines illustrate the CDF-matching technique described in the text. (bottom) The RH bias correction, which is a result of the CDF matching.

data ($0.7 \times$ KB + $0.3 \times$ LM). With weights based on their distance to EM, this approach attempts to minimize horizontal humidity variations between KB and LM. The difference in the RH CDFs of 109 contemporaneous sondes (i.e., launched within 2 h of each other) from the NCAR merged site and EM forms the basis of the differential bias correction between these sites. This method of CDF matching, which essentially forces the two sites to have similar CDFs, follows the approach taken by Nuret et al. (2008) to correct the humidity biases in AMMA sondes. As in Nuret et al. (2008), the procedure presented here uses RHs computed with respect to water at all temperatures. Because the RH bias varies in the vertical, as seen in Fig. 4, computations are performed for 20°C temperature bins between +40 and −80°C. CDFs were created in these six temperature bins by placing the 5-hPa sonde data in 5% RH intervals. Within a given temperature interval, the bias between the CDFs is computed for each percentile of the CDF in which each percentile bin contains an equal number of observations. The final correction table is created by linearly interpolating the bias from irregular RH values to uniform RH values at 1% intervals and 0% differential bias at RH = 0% and 100%.

To illustrate further how the bias correction is computed, consider the CDFs for the merged KB–LM and EM data for the temperature interval 20–40°C in Fig. 9a. The differential bias is found by matching the CDFs at a given percentile and taking their difference. An example is illustrated in Fig. 9a, in which the EM RH value of 46% at the 40th percentile is matched to the corresponding KB–LM value at this percentile, which is 50%, yielding a bias correction of 4% for an EM RH value of 46%. For the two CDFs in Fig. 9a, their differential bias over the entire range of RHs is shown in Fig. 9b. To provide a smooth transition in the bias correction between temperature intervals, the correction is linearly interpolated between temperature intervals. For example, at a temperature of 20°C, the bias would be equally weighted by the bias correction in the 20°–40°C interval with that in the 0°–20°C interval. This smooth transition is reflected in the bias-correction table shown graphically in Fig. 10. As seen in this plot, for temperatures >0°C the bias correction peaks near 10% for RH values around 30%. For temperatures <0°C, the bias correction gradually increases with colder temperatures peaking near 20% in the −60° to −80°C temperature interval for RH values between 10% and 20%. This bias correction was applied to sondes from SMN sites along the east side of the GOC, namely EM and MZ, and will be referred to as the bias correction east (BCE).

Because of drier conditions along the western side of the GOC (Fig. 7), a second bias correction was developed using contemporaneous sondes between LR (an NCAR site) and LP (an SMN site ~220 km to the south of LR). For this analysis, 136 contemporaneous sondes were available. The bias-correction table for this site pairing (not shown) has larger peak biases than BCE (with corrections up to 25% for temperature $T < -60$°C),

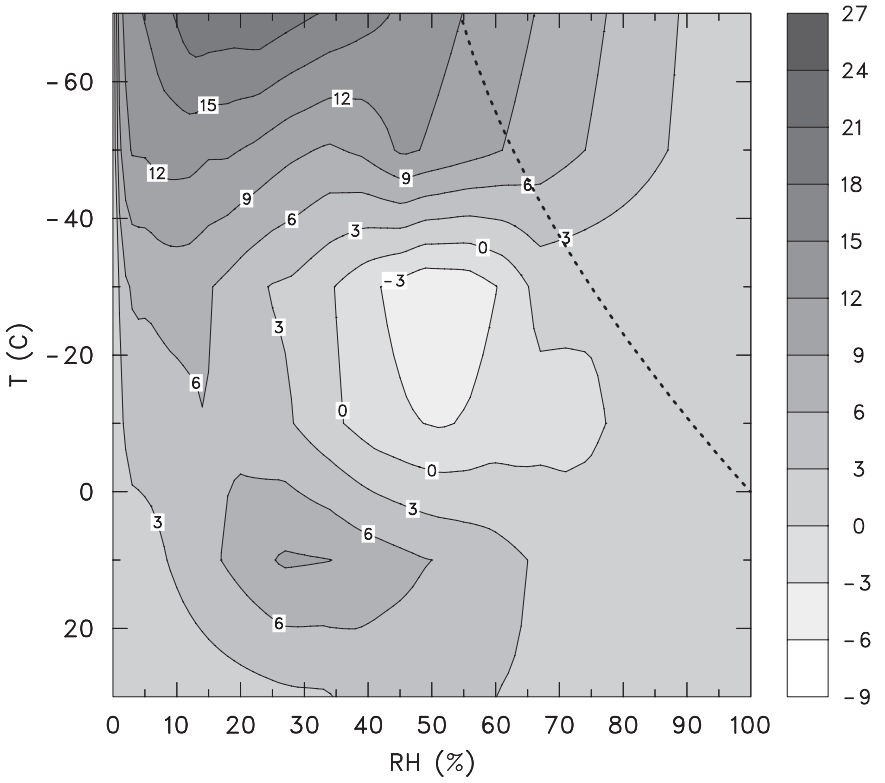

FIG. 10. Bias correction over a full range of temperatures, which was created by matching the CDFs from the KB–LM merged data to the EM data. This correction, referred to as BCE, was applied to SMN sites along the east side of the GOC (viz., EM, MZ, and inland SMN sites above 300 hPa). The dotted line represents the saturation line with respect to ice.

and a different structure for $T > 0$°C, in which peak biases of 10%–12% occur at RHs around 70%. This bias correction, referred to as bias correction west (BCW), was applied to correct humidities at LP. Because AL was about equal distance from each coast, both bias corrections (BCE and BCW) were applied to correct the AL humidities. These intermediate values were then averaged together with equal weights to determine the final corrected humidities at AL.

Although the analyses presented in Fig. 3 suggest that a correction is justified at a number of the inland SMN sites, the absence of reliable inland NCAR sites makes developing such a correction problematic. Fortunately, as discussed above, the characteristics of the low-level moisture data at TR seem quite reasonable, such that data from this site are used to develop a correction for CH, which exhibits a serious dry bias (Figs. 3, 6) and is positioned at a critical location in the core of the monsoon (CH being at a vertex of the EBA; see Fig. 1). Using 147 contemporaneous sondes from TR and CH, a bias correction inland (BCI) was developed and applied to the CH data. The bias-correction table for this site pairing (not shown) gives the largest corrections (~10%) for CH RHs between 10% and 30% and temperatures >20°C. Beyond the corrections at this inland site, inhomogeneous moisture fields over the Mexican mainland, as evidenced by large spatial gradients in PW (Kursinski et al. 2008) and surface moisture (Ciesielski and Johnson 2008), make developing a full troposphere humidity correction at the other inland SMN particularly difficult.

On the other hand, correcting the upper-level dry bias at the inland SMN sites seems more feasible. As noted in Fig. 3b, all inland SMN sites exhibit an absence of saturated layers, which occurs predominately at upper levels. In addition, comparisons of mean RH structures (not shown) between reliable U.S. sites [El Paso (EP) and Del Rio (DR)] to their nearest SMN sites (CH and MT, respectively) reveal upper-level (300 hPa and above) dry biases at these SMN sites in the range of 30% and nearly identical in vertical structure to those observed in Figs. 4 and 5. Based on these observations and the assumption that convective systems in the core monsoon region would result in frequent anvil clouds at all the inland SMN sites (Nesbitt et al. 2008), the BCE was applied to all inland SMN sites at pressure levels ≤300 hPa.

TABLE 1. Summary of CDF-matching bias corrections that were applied in this study.

Site corrected	Correction used	Comments
EM, MZ	BCE	Based on matching EM with weighted KB/LM data
LP	BCW	Based on matching LP with LR data
AL	BCW, BCE	Average of two corrections, because AL located roughly between two coasts
CH	BCI	Based on matching CH with TR data
CH, TR, MT, ZC, GD, MN	BCE	Applied for $p < 300$ hPa

Table 1 summarizes the CDF corrections that were applied in this study. Because a significant effort was previously made to improve and quality control the 5-hPa dataset as described in Johnson et al. (2007), the later dataset, rather than the native resolution sonde dataset, was used as the starting point for the corrections applied in this study. No CDF corrections were applied to the surface points, except at AL and LR (see footnote 3).

The impact of using separate day and night bias-correction tables was also examined. RH differences between NCAR and SMN sites, such as those presented in the profiles in the right-hand panels of Figs. 4 and 5, exhibited day-to-night differences on the order of a few percent (not shown). However, using separate day and night bias-correction tables had little to no impact on the final moisture analysis. For example, the fractional change in the daily mean PW at AL was 0.04%, whereas the change at different hours of the day was less than 0.5%. Because this impact was minimal on the RH analysis, correction tables based on all sonde times were used in this study. This has the added advantage of keeping the sample sizes for the bias tables larger, which minimizes the effects of random sampling errors.

b. *Daytime dry bias correction of the Vaisala RS80-H sondes*

Using comparisons between PW retrieved from a microwave radiometer and that from sonde data at the Atmospheric Radiation Measurement Project (ARM) southern Great Plains site, Cady-Pereira et al. (2008) developed a correction to r for the daytime dry bias found in different Vaisala sonde types. Despite a protective covering on the RS80-H humidity sensor to shield it from precipitation and radiative effects, the daytime dry bias is attributed to solar heating of the sonde humidity sensor. As reported in Cady-Pereira et al. (2008), later model Vaisala sondes, which lack this covering, have a more pronounced daytime bias than the RH80-H model. In their study, no attempt was made to determine a height-dependent r correction. For RS80-H sondes they give the correction as

$$\mathrm{SF} = 1.0 + 0.067 \exp[-0.2/\cos(\mathrm{SZA})], \qquad (1)$$

where SF is a scale factor that multiplies water-vapor mixing ratio r at each level and SZA is the solar zenith angle.

For each of the sounding sites in the T1A domain (see Fig. 1) that used Vaisala RS80-H sondes during NAME (four of the U.S. sites used VIZ sondes), the daytime correction scheme given in (1) was applied. As seen in this equation, the SF correction is only a function of SZA, which in turn is a function of the station's latitude and longitude position, day of the year, and time of the day. For example, Fig. 11 shows the SF correction that would be applied to humidity data at the AL site on 15 July as a function of time of day. As seen here, only sondes launched between 0730 and 1930 LT are affected, with r values from sondes launched between 1130 to 1730 LT being increased by about 5%. In practice, the daytime correction was applied by converting the dewpoint temperature T_d to an r value, scaling the r value, and then converting the scaled r value back to a new T_d. By computing this new T_d with respect to water, the magnitude of the correction in terms of RH increased somewhat with height above the freezing level. This effect was considered desirable because, in recent studies, both Vömel et al. (2007) and Yoneyama et al. (2008) found an RH dry bias that increased with height when comparing Vaisala RS92 humidities to highly accurate moisture soundings from a chill mirror hygrometer.

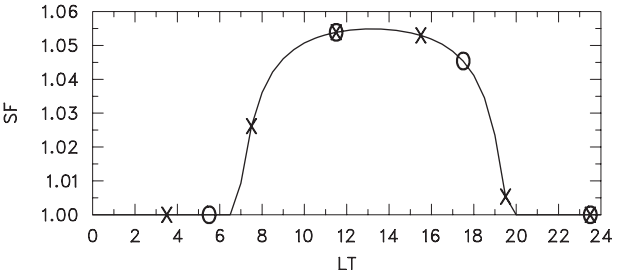

FIG. 11. Scale factor (SF) for correction of sonde water-vapor mixing ratio r as a function of local time for sondes released at the position of AL (see Fig. 1) on 15 Jul. Symbols X and O indicate the SF applied to sondes launched at 6 and 4 day^{-1} frequencies, respectively.

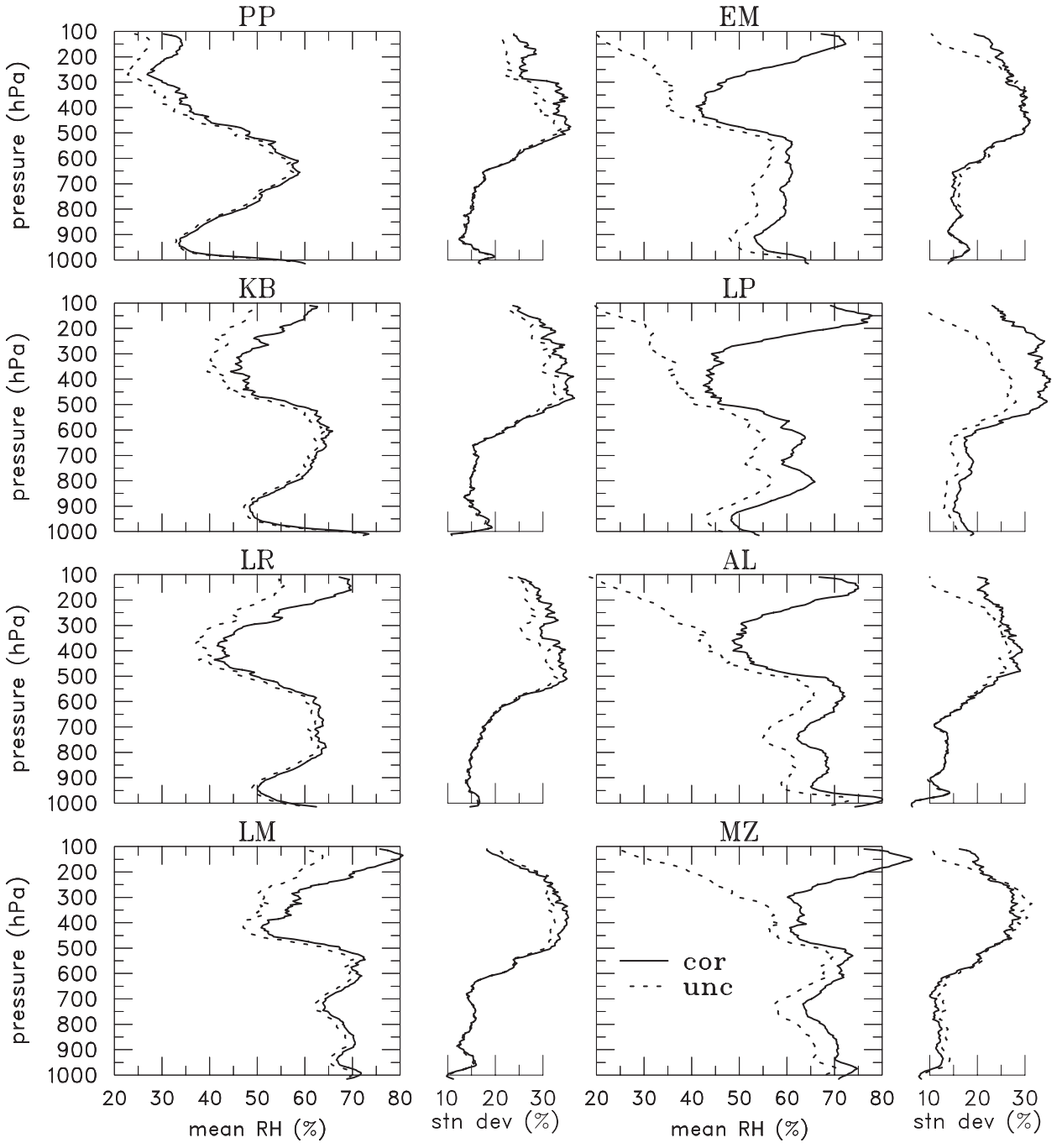

FIG. 12. Mean and standard deviation of RH (with respect to ice for $T < 0$°C) computed for sondes launched during the NAME EOP from (left) NCAR and (right) SMN sites in the GOC by using uncorrected (dashed curves) and corrected (solid curves) RH data.

4. Validation of correction

This section considers the impact of the corrections described in section 3 on various moisture analyses, as well as its effect on the properties of convection and the atmospheric moisture budget over the core of the monsoon region. All RH analyses presented in this section show RH computed with respect to ice for $T < 0$°C.

Figure 12 shows the impact of the corrections on the EOP-mean RH profiles for the eight sounding sites located in the GOC. The left panels of Fig. 12 show the mean RH profiles and their standard deviations at the

four NCAR sites. At these sites, where only the daytime solar correction is applied, one can see its effect is to increase the mean RH a few percent in the low and midtroposphere and up to 20% above 300 hPa. The most notable difference between NCAR profiles and those constructed with uncorrected SMN humidities (dashed curves on right-hand side of Fig. 12) is at the upper levels, where the SMN sites reported very low RHs. In the corrected SMN profiles (solid curves in right-hand side of Fig. 12), the upper-level RH values increase dramatically, at some levels up to 60%, and are in much better agreement with those observed at the NCAR sites. The ~80% mean RHs seen at upper levels in the corrected profiles of the southern GOC sites are similar to those observed in humidity-corrected TOGA COARE profiles (see Ciesielski et al. 2003, Fig. 2). At low and midlevels, the corrections increase the RHs from 7% to 12% with the majority of the increase a result of the CDF correction. The rapid decrease in RH above 600 hPa, seen at all the NCAR sites and noted in Johnson et al. (2007), is preserved in the SMN-corrected data.

The frequency of saturated levels in these corrected SMN sondes increases from an average of 0.3% to 3.3%, which is still less than that observed from the four corrected NCAR sites (4.9%). At the inland SMN sites, the corrections act to moisten the upper levels in a similar fashion as in the GOC SMN sites. The frequency of saturated levels at the inland SMN sites increases substantially (Fig. 3b) by using the corrected data, but it is still less than that observed at the NCAR sites. The two SMN sites in Fig. 3b [Guadalajara (GD) and Manzanillo (MN)], which showed essentially no increase in saturated layers, had only early morning (1200 UTC) sonde launches and thus were not affected by the daytime correction.

The impact of the moisture correction on AL data can be seen in more detail by examining contoured frequency by altitude diagrams (CFADs) of RH constructed without and with corrected data (Fig. 13). This format allows us to examine how corrections affect the RH distribution changes at various vertical levels. Of particular note is how the correction increases the frequency of saturation (i.e., RHs = 100%) at certain levels. For example, near 0.5 km, the correction results in a saturation frequency increase from 1% to 7%, whereas at 5.5 km the increase is from 5% to 10%. The higher frequency of saturation at these levels is consistent with ceilometer analysis during this period (see Zuidema et al. 2007, Fig. 6), which showed the occurrence of cloud bases peaking at 0.5 and 5.5 km with frequencies of 10% and 15%, respectively. This consistency corroborates the notion that the correction scheme has improved the description of the humidity field.

Although recent studies (Nuret et al. 2008; Yoneyama et al. 2008) have verified their moisture-correction scheme against PW estimates from collocated GPS receivers, this was only an option at PP, as mentioned earlier. Contemporaneous measurements showed that the sonde-mean-corrected PW value at PP of 40.1 mm was ~2.8 mm lower than the mean GPS value. The Cady-Pereira et al. (2008) correction reduced the daytime difference between sonde and GPS PW from 4 to 2 mm. The remaining 2 mm bias may be due to dislocation of the two instruments, because the daytime surface RH at the coastal GPS site was about 20% higher than that at the inland ISS site. Nighttime surface conditions show little difference between the instrument sites, so that the nighttime GPS minus sonde PW difference of 3.4 mm likely represents an actual nighttime dry bias in the sondes. The magnitude of this nighttime dry bias is larger than the mean value of 0.35 mm reported in Wang and Zhang (2008) for this type of sonde, but it is consistent with their finding that the bias is larger in dry environments. A second source for PW estimates, at least over the oceans, comes from AMSR-E data, as seen in Fig. 7, which shows its PW analysis for the NAME EOP. The humidity-corrected sonde PW estimate for AL of 52.3 mm (see Table 2) compares reasonably well to the AMSR-E estimate of 53.7 mm at the AL position. In addition, the corrected AL sonde data appears to preserve the diurnal variations in PW. For example, when only AL sondes launched within three hours of the AMSR-E overpass times of 0300 and 1500 LT are considered, the corrected PW estimates are 53.6 and 52.3 mm, respectively, as compared to the satellite estimates of 54.9 and 52.7 mm. Similar to PP, the dry bias in the corrected sondes is larger at night (−1.3 mm versus −0.4 mm for daytime sondes). It is also worth noting that the higher PW values at 0300 LT are consistent with the findings of Zuidema et al. (2007), which showed a nighttime peak in RH and clouds at AL. Although the corrected AL sonde PW values are about 1 mm too low compared to the satellite estimates, they nevertheless represent a considerable improvement over the uncorrected data, as seen in Table 2, which also shows the PW values (uncorrected and corrected) for the NCAR and other SMN sites in the GOC region. Use of the CDF corrections increased the PW at the GOC SMN sites (indicated with an asterisk in Table 2) by an average of 4.8 mm. The impact of the daytime correction on PW was smaller, increasing the mean PW at all sites by ~1 mm. Viewed collectively, the PW estimates using corrected data exhibit much better spatial continuity among the sites, as noted in Table 2. In particular, the PW differences between EM and its adjacent sites are greatly reduced by using the corrected data.

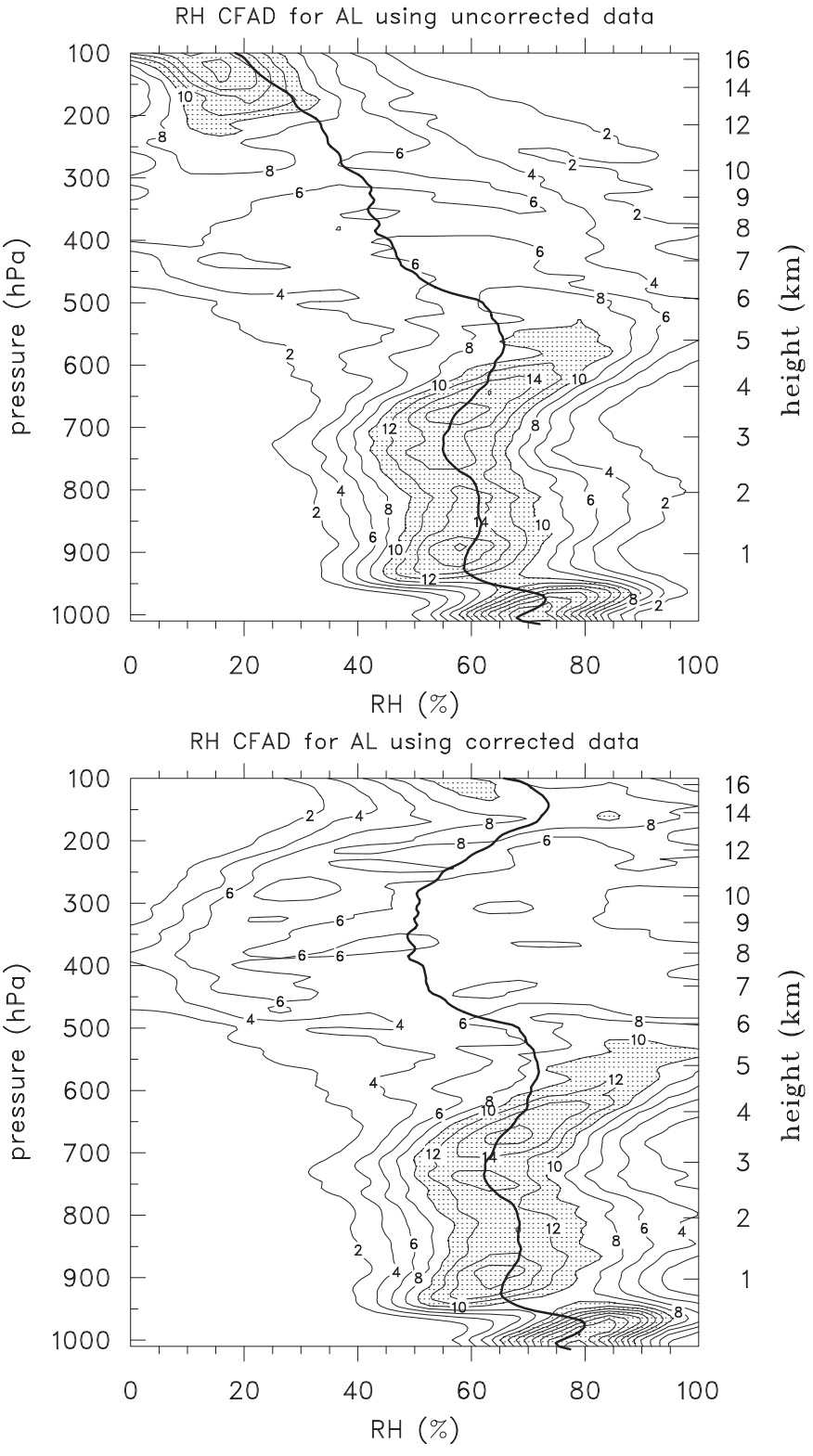

FIG. 13. RH CFADs constructed from (top) uncorrected and (bottom) corrected data for AL by using 152 sondes during the NAME EOP. The contour interval is 2% with values greater than 10% shaded. The heavy solid line represents the mean RH. In this analysis, RH values were computed with respect to ice for temperatures ≤0°C.

TABLE 2. Values of PW, CAPE, and CIN for NCAR and SMN sites averaged over the NAME EOP. Uncorrected values are in parentheses. Sites are ordered from north to south within regions.

Sounding site (type, No. of sondes)	PW (mm)	CAPE (J kg^{-1})	CIN (J kg^{-1})
West side of GOC			
LR (NCAR, 175)	(45.8) 47.1	(594) 732	(−446) −418
LP (SMN, 155)*	(39.3) 44.9	(14) 134	(−473) −397
Central GOC			
AL (SMN, 151)*	(46.9) 52.3	(637) 1393	(−285) −179
East side of GOC			
PP (NCAR, 121)	(39.0) 40.1	(648) 807	(−678) −653
KB (NCAR, 120)	(47.9) 49.2	(1419) 1595	(−398) −377
EM (SMN, 140)*	(44.4) 49.2	(613) 1125	(−454) −401
LM (NCAR, 206)	(52.7) 54.1	(1197) 1397	(−261) −238
MZ (SMN, 146)*	(49.4) 52.9	(680) 1109	(−255) −191
East side of SMO			
CH (SMN, 149)*	(22.3) 25.2	(17) 201	(−374) −362
TR (SMN, 143)	(27.7) 28.3	(36) 52	(−425) −408

* SMN sites corrected with the CDF-matching procedure throughout the entire depth of the troposphere.

Although the correction scheme produces the largest RH increases at upper levels, as seen in Fig. 12, the largest increases in terms of actual moisture amount r occur in the lowest levels. For example, in the lowest 50 hPa, the corrected data increase the water vapor mixing ratio by 1.3 g kg^{-1} when averaged over the four GOC SMN sites. Because of the strong sensitivity of convection to the low-level thermodynamic field (e.g., Crook 1996), Table 2 shows the impact of the corrections on convective available potential energy (CAPE) and convective inhibition (CIN). Here CAPE and CIN values were calculated assuming pseudoadiabatic ascent of a parcel with mean thermodynamic conditions representative of the lowest 50 hPa. The NCAR sites, which were corrected for the daytime dry bias, show an average CAPE increase of 164 J kg^{-1} and a |CIN| decrease of 24 J kg^{-1}. The change in these parameters at the GOC SMN sites, which had both the daytime and CDF corrections, was considerably larger: CAPE increased 454 J kg^{-1} and |CIN| decreased by 75 J kg^{-1}. Although not shown in Table 2, the lifting condensation level (LCL) at these SMN sites lowers 18 hPa on average and the level of neutral buoyancy rises 35 hPa because of the corrections. The changes of PW and in the convective parameters at the SMN GOC sites are of the same magnitude as those found from correcting the dry bias in the Vaisala RS80-H sondes in TOGA COARE (Ciesielski et al. 2003). Overall, use of the corrected data produces much smaller and more realistic differences in the convective parameters between adjacent sites.

One of the motivations for correcting the SMN moisture data was to improve the description of the humidity field within the context of a gridded objective analysis. An important aspect of this gridded dataset is that it is largely independent of model data[4] and thus not affected by issues with model parameterization schemes. As such, these objective analyses are useful for model and reanalysis validation, model initialization, and defining large-scale forcing fields as input to cloud-resolving and single-column models. We now consider how the moisture correction impacts various analyses derived from the objective gridded dataset. This dataset—at 1° horizontal resolution, 25 hPa vertical resolution, and 4 times daily for the NAME EOP—covered the area from 15°–35°N, 115°–100°W. Johnson et al. (2007) describe the details of how these gridded datasets were created. In considering the moisture-correction impacts, one should keep in mind that objective analysis schemes, such as the one used here, inherently smooth out large gradients between adjacent sites so that biases between sites are somewhat diminished by the smoothing properties of the analysis scheme. For example, the actual difference between the 150-hPa mean uncorrected RHs at EM and LM is 38% in Fig. 12, whereas in the gridded dataset this difference for the same period is only 20%.

To verify that the humidity corrections produced an improvement in the gridded analysis, Table 3 shows a comparison of the uncorrected and corrected gridded r field to 1-min averaged aircraft data collected from the 10 WP-3D flights during NAME. To ensure the most reliable comparison, only aircraft data that fell within EBA domain (see Fig. 1) and within ±2 h of a grid analysis time were used. When these criteria were satisfied, the gridded analyses were interpolated to the location of the aircraft observation and the difference was determined. Mean differences for three analysis times (0600, 1200, and 1800 LT; the aircraft having no night flights) are listed in Table 3 for various levels of correction. The average pressure level for these comparisons is 871 hPa. With only the CDF correction, the daytime dry bias is still quite prominent. The daytime correction further reduces but does not completely remove the dry bias. For reasons unclear at this time, the gridded analyses also show a cool bias of 0.73°C relative to the aircraft data. Taking this factor into account (because r is also a function of temperature) further reduces the mean dry bias of the gridded analyses to 0.3 g kg^{-1}, which arises primarily from 1200 LT analysis times. These comparisons with independent aircraft data, albeit limited to the lower troposphere, give us

[4] Although model reanalysis was used over data-sparse regions of the eastern Pacific to help the analysis, sensitivity tests show that this use of model data has little, if any, impact on the analysis over the GOC and land areas.

TABLE 3. Comparison of gridded r analyses to WP-3D aircraft data. Numbers represent the average difference $r_{\text{gridded}} - r_{\text{aircraft}}$. Column labels denote the following: unc denotes uncorrected gridded data, cor_{CDF} denotes CDF-corrected data, and $\text{cor}_{\text{DYF+DAY}}$ denotes CDF- and daytime-corrected data. The last column uses $\text{cor}_{\text{DYF+DAY}}$ data with the temperature bias removed. See text for more details. Negative numbers indicate that the gridded analysis is dry relative to the aircraft data.

Time	No. of comparisons	unc	cor_{CDF}	$\text{cor}_{\text{CDF+DAY}}$	$\text{cor}_{\text{CDF+DAY}}$ (T bias removed)
0600 LT	190	−1.0	−0.2	−0.2	+0.4
1200 LT	339	−2.5	−1.8	−1.4	−0.8
1800 LT	157	−1.7	−1.1	−0.6	+0.1
Mean	686	−1.9	−1.2	−0.9	−0.3

confidence that the corrections have substantially improved the analysis of the moisture field.

The effects of the moisture corrections on the gridded dataset are shown in Fig. 14, where a cross section perpendicular to the GOC (see Fig. 1) and constructed from only 1800 LT analysis times, is presented without (Fig. 14, top) and with (Fig. 14, bottom) corrected humidities. Also shown here is the wind field in the plane of the cross section, which shows upslope flows along both sides of the SMN with deep upward vertical motion above the western slopes of the SMO. This vertical motion field results in deep heating and a diurnal maximum in rainfall near this hour and over the western slopes of the SMO (Gochis et al. 2007; Lang et al. 2007). Using the corrected data gives a more reasonable depiction of the humidity field with deep moisture over the western slopes of the SMO and near-saturated conditions in the upper-level outflow layer, where anvil clouds are common at this time of day. In reality, near-saturated RHs likely exist throughout the depth of the troposphere over the SMO at this time, which are associated with the deep convection that occurs there during the late-afternoon and evening hours. However, without any sounding sites over the higher elevations of the SMO, the analyses over this region represent an interpolation of sondes between coastal locations and sites well east of the SMO crest (i.e., CH and TR).

Finally, we examine the impact of the humidity corrections on gridded fields averaged over the core of the monsoon region, namely the EBA shown in Fig. 1. It is over this region that the sonde density and frequency (4–6 day^{-1}) were highest and the analyses are most frequently used. Using the 4 day^{-1} gridded analyses described above, Fig. 15 shows the vertical profiles of RH, r, and the apparent moisture sink Q_2 averaged over the land and gulf portions of the EBA. Here, Q_2 is defined as $-L(\partial\overline{r}/\partial t + \overline{\mathbf{v}}\cdot\nabla\overline{r} + \overline{\omega}\partial\overline{r}/\partial p)$, where $\mathbf{v}$ is the horizontal velocity, ω the vertical p velocity, and L the latent heat of vaporization. Taking the vertical integral of Q_2 results in the following relationship: $\langle Q_2\rangle = L(P - E)$, where $\langle\cdot\rangle$ denotes the vertical integral, P denotes the precipitation rate, and E denotes the evaporation rate.[5] Although overall humidity increases are slightly larger over the gulf EBA because of the corrections, both regions show roughly a 5% increase in RH at low levels to about a 50% increase at 150 hPa. In terms of actual moisture, the correction results in r increase 0.6–0.8 g kg^{-1} over the lower troposphere.

Although changes in the time-mean Q_2 resulting from the correction are small and subtle, the structure of the Q_2 profiles over these adjacent regions is markedly different. Over the gulf, strong low-level subsidence (Fig. 14) results in large apparent moistening rates, which peak in the boundary layer (Fig. 15, top panel). In contrast, rising motion over the land EBA (Fig. 14) results in apparent drying at most levels (Fig. 15, bottom panel). Some moistening is observed between the freezing level (near 560 hPa) and 750 hPa, likely resulting from the evaporation of rain under stratiform anvils. Over the gulf EBA, the correction results in less low-level (below 950 hPa) moistening, which seems plausible because a moister environment would lessen evaporative effects. The $\langle Q_2\rangle$ over the gulf decreases slightly from −34 to −37 W m^{-2} implying a reduction in P of 0.1 mm day^{-1}. Over land, the $\langle Q_2\rangle$ increases from 65 to 71 W m^{-2}, implying an increase in P of 0.2 mm day^{-1}. These changes in $\langle Q_2\rangle$ and P are smaller than that observed over the TOGA COARE intensive flux array (IFA), in which P increased 0.5 mm day^{-1} because of humidity corrections. In TOGA COARE, the larger impact of the humidity correction on P was primarily due to changes in the horizontal advection of r. This, in turn, resulted from changes in the horizontal r gradient, because sites in the IFA experienced a moisture increase while sites to the north experienced a moisture decrease. In NAME, the correction increased the moisture at all sites, which resulted in little impact on horizontal moisture gradients.

Although the humidity corrections had minimal impact on the time-mean Q_2, its diurnal cycle shows considerable change, as seen in Fig. 16. In the uncorrected analysis, $\langle Q_2\rangle$ peaks at 1200 LT, which implies maximum rainfall at this time. In the corrected version, $\langle Q_2\rangle$ is quite small at 1200 LT and peaks at 1800 LT, which is consistent with the diurnal cycle of rainfall in this area

[5] Unfortunately, the scarcity of reliable estimates of E over the land EBA made it difficult to compute P as a budget residual.

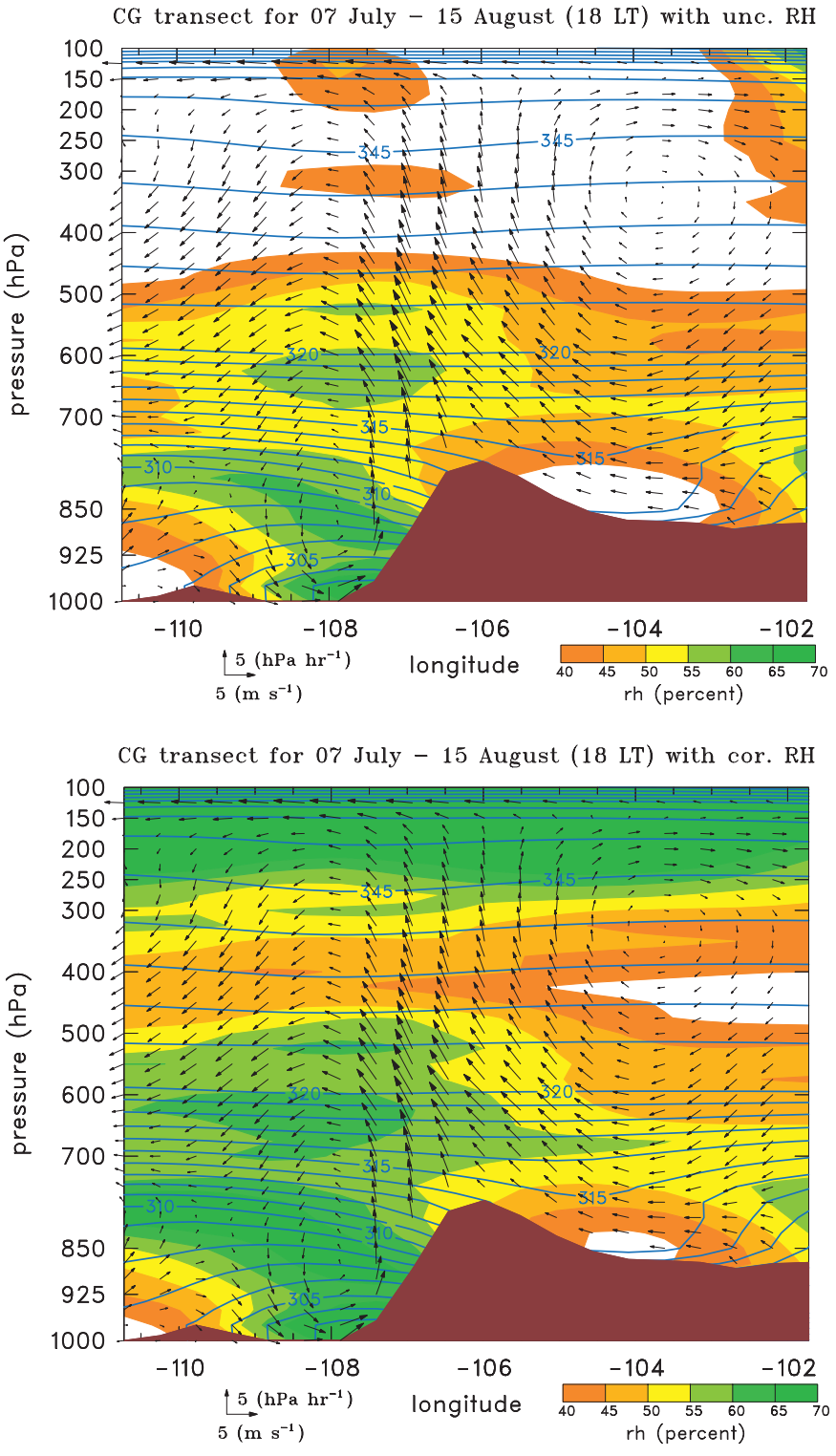

FIG. 14. CG transect (position shown in Fig. 1) of RH (shaded contours with scale at bottom) with (top) uncorrected and (bottom) corrected RH data averaged over the period from 7 Jul to 15 Aug 2004 using only 1800 LT times. Blue lines are isentropes and arrows denote wind flow in the plane of transect (scale shown at bottom). White areas indicate RHs $< 40\%$.

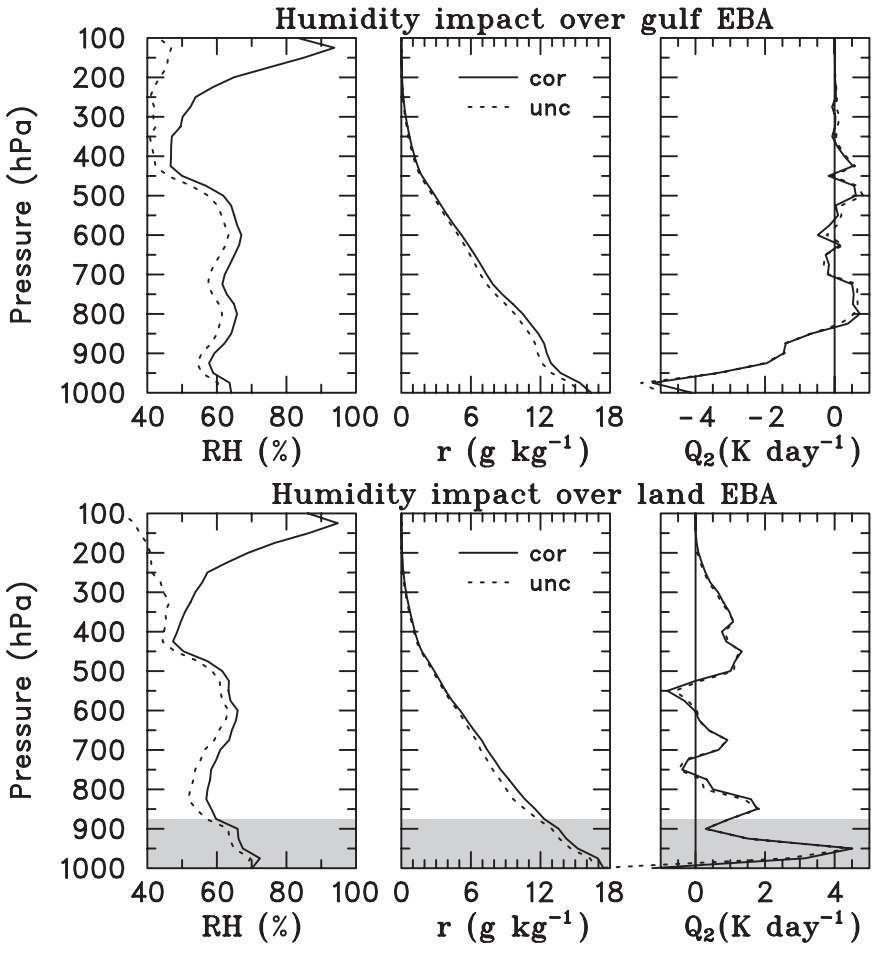

FIG. 15. Impact of the humidity correction on gridded analyses averaged over the (top) gulf and (bottom) land portions of the EBA shown in Fig. 1. EOP-mean vertical profiles for (left)–(right) RH, r, and apparent drying Q_2. Analyses using uncorrected data are shown with dashed curves, with corrected data in solid curves. Shading in land-EBA plots indicates that some of the land area was below ground at these pressure levels.

(Gochis et al. 2007). This dramatic change in the diurnal cycle of Q_2 is primarily the result of the daytime humidity correction and its impact on the local tendency term ($\partial\bar{r}/\partial t$) when computing Q_2.

5. Summary and concluding remarks

During the North American Monsoon Experiment (NAME) from 7 July to 15 August 2004, the upper-air sounding network over northwestern Mexico and the southwestern United States was enhanced by increasing the frequency of sonde launches and adding five sites in the Gulf of California (GOC). Four of these additional sites were maintained and operated by NCAR. Postprocessing of the sondes revealed that data from several of the SMN sites operated by Mexico had a significant dry bias relative to the NCAR sites, despite the fact that all the sites within the core monsoon region used the same sonde type (i.e., Vaisala RS80-H). This paper describes the corrections applied to the moisture variable in the NAME upper-air sounding dataset and examines how these corrections impacted various analyses.

Two different correction procedures were applied to the sonde moisture variable for sites in the NAME domain. The first procedure, referred to as the CDF correction, attempted to match the statistical properties of an SMN site with questionable data to that of a nearby site with good data (typically an NCAR site). This procedure was applied to correct the data at all pressure levels at five SMN sites and above 300 hPa at six inland SMN sites, as summarized in Table 1. The reasons for the dry bias at these SMN sites is unclear but are likely related to poor prelaunch procedures or outdated ground station software. The second procedure,

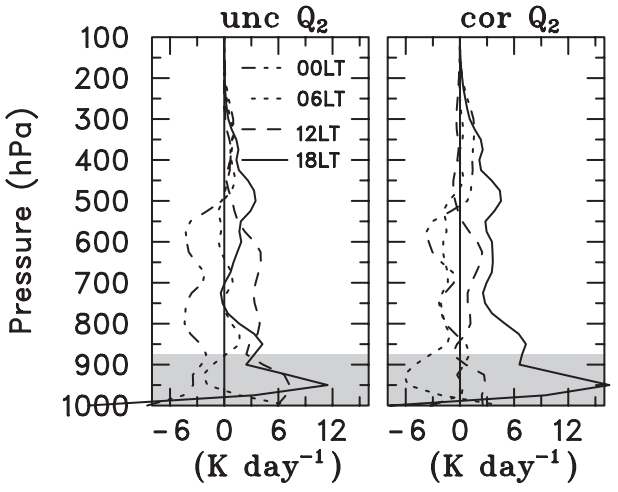

FIG. 16. Diurnal cycle of Q_2 computed using (left) uncorrected and (right) corrected humidity data for land-EBA area. Shading indicates that some of the land area was below ground at these pressure levels.

referred to as the daytime correction, was designed to remove a daytime dry bias resulting from solar heating of the humidity sensor. This later correction was applied to all 24 Vaisala RS80-H sites in the NAME domain.

The primary impacts of the corrections are as follows:

- At the GOC SMN sites, the EOP-mean RH increased from 7% to 12% below 300 hPa and from 50% to 60% near 150 hPa. Corrected humidity data from these sites are in much better agreement with nearby, more reliable NCAR sites.
- Precipitable water (PW) analysis over the GOC with corrected data shows much better spatial continuity and better agreement with independent satellite analysis. For example, the corrections increase sonde-estimated PW at the R/V *Altair,* located near the mouth of the GOC during NAME, about 12% from 46.9 to 52.3 mm compared to an AMSR-E estimate at this location of 53.7 mm.
- Comparison of the corrected gridded data to low-level humidity measurements from 10 daytime aircraft missions show that the dry bias has been substantially reduced (from 1.9 to 0.3 g kg^{-1}). Evidence for the remaining slight dry bias is also present in PW sonde comparisons with independent data, particularly in nighttime sondes.
- The corrections greatly increase upper-level RHs so that the frequency of saturated layers is more representative of a monsoon environment where frequent anvil clouds exist associated with the development and decay of mesoscale convective systems.
- In terms of water vapor mixing ratio r, the corrections produce the largest increases in the lower troposphere: about 1 g kg^{-1} at the GOC SMN sites. Because of convection's strong sensitivity to low-level moisture, the convective parameters at the GOC SMN sites show significant changes, with CAPE increasing by 450 J kg^{-1} and |CIN| decreasing by 75 J kg^{-1}. Use of the corrected data produces much better consistency in these parameters between adjacent SMN and NCAR sites.
- Use of the corrected data has a small impact on the time-mean apparent drying profile Q_2, which implies a moisture budget residual rainfall P increase over the land EBA of 0.2 mm day^{-1}. On the other hand, the impact on the diurnal cycle of Q_2 is significant, shifting the peak of P from 1200 LT, using uncorrected analyses, to 1800 LT, using corrected analyses, which is consistent with observations of precipitation in this region.

Based on the comparison of several analyses with and without the humidity corrections, we contend that the corrected dataset described herein has resulted in a much improved large-scale analysis of the moisture field for NAME EOP. These improvements should lead to more accurate simulations of convection and large-scale circulations in global models, as well as in cloud-resolving and single-column model simulations. A recent study comparing the North American Regional Reanalysis (NARR) surface fields to observations over the NAME domain showed a significant cool and dry bias in the reanalysis surface fields, which appears to impact the diurnal cycle of convection (Ciesielski and Johnson 2008). Use of the humidity-corrected data with a new reanalysis should lead to improvements in these issues in NARR. To encourage the use of this improved dataset, our gridded T1A analysis and the land-EBA large-scale forcing dataset computed with the corrected data, as described in this paper, have been made available on the Internet (available online at http://tornado.atmos.colostate.edu/name/).

Acknowledgments. This research has been supported by the National Aeronautics and Space Administration under Grant NNX07AD35G, the National Oceanic and Atmospheric Administration under Grant NA17RJ1228, and the National Science Foundation under Grants ATM-06639461 and ATM-0340602. We thank Andy Neuman for providing us the IR brightness temperature at the NCAR sites, José Meitín and Art Douglass for their investigative work in trying to determine sonde types and launch procedures, and Dr. Wes Terley for insightful discussion concerning various ways to approach the bias-correction problem.

REFERENCES

Bevis, M., S. Businger, T. A. Herring, C. Rocken, R. A. Anthes, and R. H. Ware, 1992: GPS meteorology: Remote sensing of atmospheric water vapor using the global positioning system. *J. Geophys. Res.,* **97,** 15 787–15 801.

Bock, O., M.-N. Bouin, A. Walpersdorf, J. P. Lafore, S. Janicot, F. Guichard, and A. Agusti-Panareda, 2007: Comparison of ground-based GPS precipitable water vapour to independent observations and NWP model reanalyses over Africa. *Quart. J. Roy. Meteor. Soc.,* **133,** 2011–2027.

Cady-Pereira, K. E., M. W. Shepherd, D. D. Turner, E. J. Mlawer, S. A. Clough, and T. J. Wagner, 2008: Improved daytime column-integrated precipitable water vapor from Vaisala radiosonde humidity sensors. *J. Atmos. Oceanic Technol.,* **25,** 873–883.

Ciesielski, P. E., and R. H. Johnson, 2008: Diurnal cycle of surface flows during 2004 NAME and comparison to model reanalysis. *J. Climate,* **21,** 3890–3913.

——, ——, P. T. Haertel, and J. Wang, 2003: Corrected TOGA COARE sounding humidity data: Impact on diagnosed properties of convection and climate over the warm pool. *J. Climate,* **16,** 2370–2384.

Crook, N. A., 1996: Sensitivity of moist convection forced by boundary layer processes to low-level thermodynamic fields. *Mon. Wea. Rev.,* **124,** 1767–1785.

Gochis, D. J., C. J. Watts, J. Garatuza-Payan, and J. Cesar-Rodriguez, 2007: Spatial and temporal patterns of precipitation intensity as observed by the NAME event rain gauge network from 2002 to 2004. *J. Climate,* **20,** 1734–1750.

Guichard, F., D. Parsons, and E. Miller, 2000: Thermodynamic and radiative impact of the correction of sounding humidity bias in the tropics. *J. Climate,* **13,** 3611–3624.

Higgins, W., and Coauthors, 2006: The NAME 2004 field campaign and modeling strategy. *Bull. Amer. Meteor. Soc.,* **87,** 79–94.

Johnson, R. H., P. E. Ciesielski, B. D. McNoldy, P. J. Rogers, and R. K. Taft, 2007: Multiscale variability of the flow during the North American Monsoon Experiment. *J. Climate,* **20,** 1628–1648.

Kursinski, E. R., and Coauthors, 2008: Water vapor and surface observations in northwestern Mexico during the 2004 NAME Enhanced Observing Period. *Geophys. Res. Lett.,* **35,** L03815, doi:10.1029/2007GL031404.

Lang, T. J., D. A. Ahijevych, S. W. Nesbitt, R. E. Carbone, S. A. Rutledge, and R. Cifelli, 2007: Radar-observed characteristics of precipitating systems during NAME 2004. *J. Climate,* **20,** 1713–1733.

Lorenc, A., D. Barker, R. Bell, B. Macpherson, and A. Maycock, 1996: On the use of radiosonde humidity observations in midlatitude NWP. *Meteor. Atmos. Phys.,* **60,** 3–17.

Nesbitt, S. W., D. J. Gochis, and T. J. Lang, 2008: The diurnal cycle of clouds and precipitation along the Sierra Madre Occidental observed during NAME-2004: Implications for warm season precipitation estimation in complex terrain. *J. Hydrometeor.,* **9,** 728–743.

Nuret, M., J.-P. Lafore, O. Bock, F. Guichard, A. Agusti-Panareda, J.-B. N'Gamini, and J.-L. Redelsperger, 2008: Correction of humidity bias for Vaisala RS80-A sondes during AMMA 2006 observing period. *J. Atmos. Oceanic Technol.,* **25,** 2152–2158.

Rocken, C., T. Van Hove, J. Johnson, F. Solheim, R. Ware, M. Bevis, S. Chiswell, and S. Businger, 1995: GPS/STORM—GPS sensing of atmospheric water vapor for meteorology. *J. Atmos. Oceanic Technol.,* **12,** 468–478.

Stull, R. B., 1988: *An Introduction to Boundary Layer Meteorology*. Kluwer Academic, 666 pp.

Vömel, H., and Coauthors, 2007: Radiation dry bias of the Vaisala RS92 humidity sensor. *J. Atmos. Oceanic Technol.,* **24,** 953–963.

Wang, J., and L. Zhang, 2008: Systematic errors in global radiosonde precipitable water data from comparisons with ground-based GPS measurements. *J. Climate,* **21,** 2218–2238.

——, H. L. Cole, D. J. Carlson, E. R. Miller, K. Beierle, A. Paukkunen, and T. K. Laine, 2002: Corrections of humidity measurement errors from the Vaisala RS80 radiosonde—Application to TOGA COARE data. *J. Atmos. Oceanic Technol.,* **19,** 981–1002.

Wentz, F. J., 1997: A well-calibrated ocean algorithm for special sensor microwave/imager. *J. Geophys. Res.,* **102,** 8703–8718.

Yoneyama, K., M. Fujita, N. Sato, M. Fujiwara, Y. Inai, and F. Hasebe, 2008: Correction for radiation dry bias found in RS92 radiosonde data during the MISMO field experiment. *SOLA,* **4,** 13–16.

Zuidema, P., C. Fairall, L. M. Hartten, J. E. Hare, and D. Wolfe, 2007: On the air–sea interaction at the mouth of the Gulf of California. *J. Climate,* **20,** 1649–1661.